PAPER • OPEN ACCESS

Structure of Krypton Isotopes using the Generalised Bohr Hamiltonian Method

To cite this article: David Muir *et al* 2020 *J. Phys.: Conf. Ser.* **1643** 012147

View the article online for updates and enhancements.
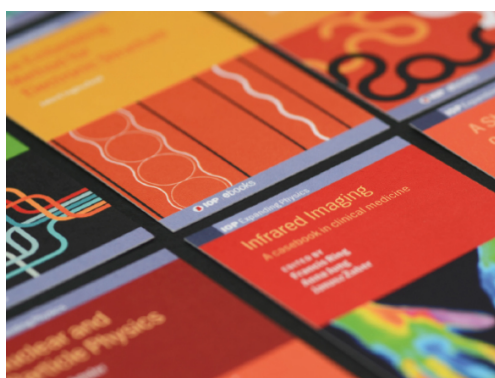
Structure of Krypton Isotopes using the Generalised Bohr Hamiltonian Method

David Muir[1]**, Leszek Próchniak**[2]**, Alessandro Pastore**[1]**, Jacek Dobaczewski**[1,3,4]

[1]Department of Physics, University of York, Heslington, York, Y010 5DD, United Kingdom
[2]Heavy Ion Laboratory, University of Warsaw, Warsaw, Poland
[3]Helsinki Institute of Physics, P.O. Box 64, 00014 University of Helsinki, Finland
[4]Institute of Theoretical Physics, Faculty of Physics, University of Warsaw, ul. Pasteura 5, PL-02093 Warsaw, Poland

E-mail: `davidmuir.physics@gmail.com`

27 September 2019

Abstract. We investigate the properties of the excited spectra of the even-even isotopes of krypton using a Generalised Bohr Hamiltonian with three different Skyrme functionals. In particular, we investigate the evolution of the low-lying 2_1^+ and 4_1^+ states and their associated electromagnetic transitions. The model reproduces quite nicely the energy trends apart from ^{88}Kr, where none of the interactions used here are able to grasp a sudden change in the energy spectrum. Additionally, we explore the neutron deficient region $^{72-76}$Kr which is a proposed region for shape coexistence. We observe that the model can reproduce the structure of the experimental spectrum of ^{72}Kr exceedingly well.

1. Introduction

Nuclear Energy Density Functional (NEDF) is the tool of choice to describe properties of atomic nuclei from light to heavy and from proton to neutron drip-lines [1]. The current functionals have reached quite high accuracy in reproducing both ground state properties such as masses [2, 3], as well as some features of the excited spectrum [4, 5, 6].

The NEDF is typically formulated to describe nuclear properties in the intrinsic reference frame of the nucleus, thus allowing for the possibility of breaking symmetries like angular momentum or particle number [7]. To compare the prediction of the model with the experimental measurement, one has to pass from the intrinsic to the laboratory frame where all these symmetries are restored. A valid alternative to an explicit process of symmetry restoration [1], is represented by the Generalized Bohr Hamiltonian (GBH) [8] method. Since GBH is a scalar under rotations and, thus, its eigenstates have good angular momentum.

The GBH has been derived microscopically and linked to an underlying mean-field calculation. For more extensive reviews see for examples Refs [9, 10, 11]. Although the GBH takes into account only quadrupole degrees of freedom, it is well suited to describe the rotation-vibration coupling, which is important to describe the spectra of a large set of nuclei. Compared to other more sophisticated methods such as the Generator Coordinate Method (GCM) [12], the GBH has the enormous advantage of being able to use as input *any* type of functional independently

on the presence of density dependent terms or not [13] and it is thus free from issues related to self-interaction or poles.

In this article, following the work done in Ref. [14], we present the GBH method using, as a microscopic input, the NEDF calculations obtained using a family of Skyrme functionals [15]. In particular, we examine the properties of the low-lying 2^+_1 and 4^+_1 states in krypton isotopes as well as their electromagnetic transitions. These nuclei have received a lot of attention both theoretically and experimentally [16, 17, 18, 19], due to shape coexistance [20] of oblate and prolate deformations in their ground states, but also to a possible modification of the N=40 shell gaps around ^{76}Kr.

2. Generalised Bohr Hamiltonian

In order to describe quadrupole collective excitations of nuclei, we use the 5-dimensional Generalised Bohr Hamiltonian [21]. The GBH is capable of describing mixtures of rotational and vibrational motions which arise in quadrupole deformed systems. It takes the form

$$\hat{H}_{coll} = \hat{T}_{vib} + \hat{T}_{rot} + \hat{V}(\beta, \gamma) \ , \tag{1}$$

where

$$\hat{T}_{\text{vib}} = -\frac{1}{2\sqrt{wr}} \left\{ \frac{1}{\beta^4} \left[\partial_\beta \left(\beta^4 \sqrt{\frac{r}{w}} B_{\gamma\gamma} \right) \partial_\beta - \partial_\beta \left(\beta^3 \sqrt{\frac{r}{w}} B_{\beta\gamma} \right) \partial_\gamma \right] \right.$$
$$\left. + \frac{1}{\beta \sin(3\gamma)} \left[-\partial_\gamma \left(\sqrt{\frac{r}{w}} \sin(3\gamma) B_{\beta\gamma} \right) \partial_\beta + \frac{1}{\beta} \partial_\gamma \left(\sqrt{\frac{r}{w}} \sin(3\gamma) B_{\beta\beta} \right) \partial_\gamma \right] \right\} \ , \tag{2}$$

$$\hat{T}_{\text{rot}} = \frac{1}{2} \sum_{k=1}^{3} \frac{I_k^2(\Omega)}{4 B_k(\beta, \gamma) \beta^2 \sin^2(\gamma - 2\pi k/3)}. \tag{3}$$

$\hat{V}(\beta, \gamma)$ is the potential energy of the nucleus and I_k denotes the k-component of the angular momentum in the body-fixed frame of a nucleus. All these quantities are parametrised in terms of the deformation parameters β and γ and of 6 mass parameters B. In the previous expressions, we also used the shorthand notations $w = B_{\beta\beta}B_{\gamma\gamma} - B_{\beta\gamma}^2$ and $r = B_x B_y B_z$.

According to Ref. [14], the potential energy surface $\hat{V}(\beta, \gamma)$ as well as the 6 mass parameters have been calculated solving the Hartree-Fock-Bogoliubov (HFB) equations for a set of parameters β, γ. In the present article, we use the HFODD solver [22] in Cartesian coordinates, to calculate the potential energy surface solving the constrained HFB equations at various β, γ points. The calculations are performed using a deformed harmonic oscillator basis with 16 major shells. We have checked that this value is rich enough to adequately converge both the energy and electromagnetic transitions of excited states. The mass parameters are calculated via the cranking approximation [23, 24]. To take into account the neglecting of time odd fields in such approximations, we uniformly rescale the 6 mass parameters by a factor of 1.3 in all following calculations. For more detailed discussion on the GBH we refer to Ref. [14].

To perform the calculations we make use of 3 Skyrme functionals: UNEDF0 [25], UNEDF1 [26] and UNEDF1$_{SO}$ [27]. Since these functionals have been adjusted on open shell nuclei, the parameters of the pairing sector are fixed. Although these functionals belong to the same family, they have been adjusted using slightly different fitting protocols and, as discussed below, they provide quite different deformation patterns in Kr isotopes.

3. Results

In Fig. 1, we show the evolution of energies of the 2^+_1 and 4^+_1 states along the Kr isotopic chain obtained for the different functionals. We observe that the trend of the 2^+_1 is fairly well
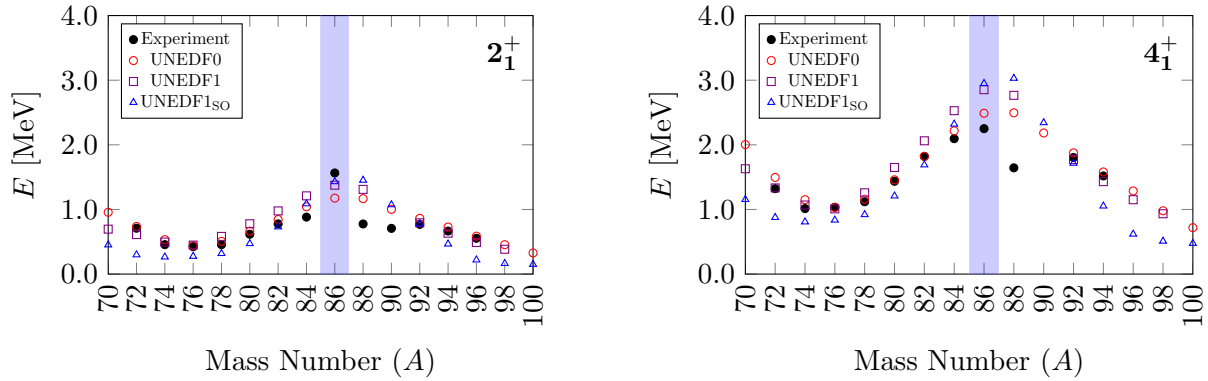
Figure 1. (Colour Online) We represent the evolution of the energies expressed in MeV of the first excited 2_1^+ (left panel) and 4_1^+ (right panel) states across the krypton isotopic chain for the 3 functionals: UNEDF0 represented by hollow circles; UNEDF1 represented by hollow squares and UNEDF1$_{SO}$ represented by hollow triangles and compare them to the experimental results [28] represented by the solid dots. The light blue bands highlight the semi-magic ^{86}Kr nucleus.
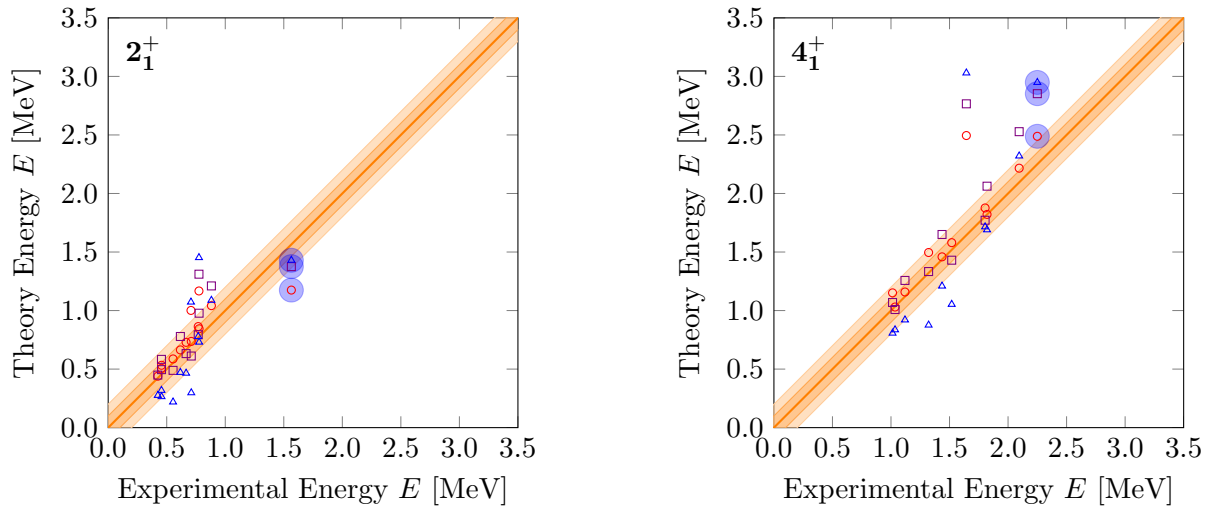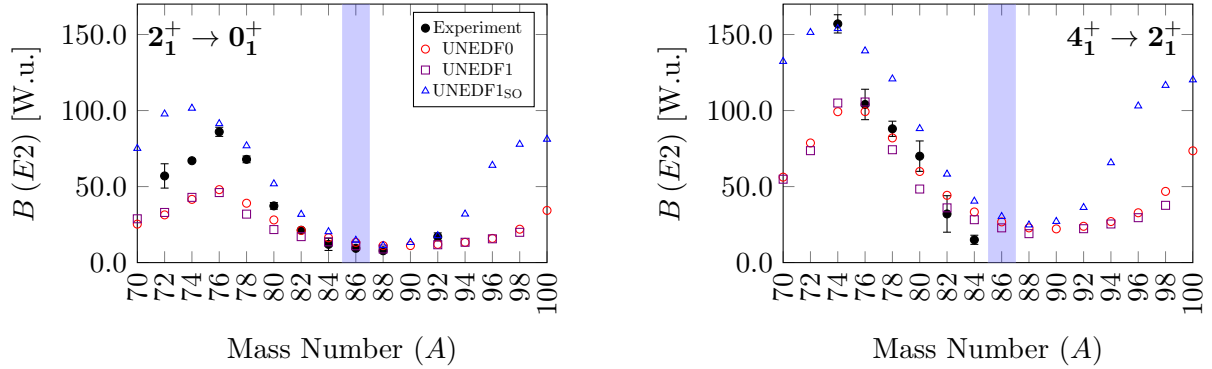

Figure 2. (Colour Online) Shows the first 2_1^+ (left panel) and 4_1^+ (right panel) theoretical energy states against the corresponding experimentally measured states [28] for all 3 UNEDF functionals represented by hollow: circles for UNEDF0; squares for UNEDF1 and triangles for UNEDF1$_{SO}$. To guide the eye we add errorbars of ± 100 keV (inner bound) and ± 200 keV (outer bound). Highlighted in large circles are the semi-magic ^{86}Kr nuclei.

reproduced by all functionals, with an energy increase around the shell closure at $N = 50$. A similar good agreement was also shown in Refs [17, 19] also based on similar GBH methods but using different functionals. The evolution of 4_1^+ states is also fairly well reproduced in the region $^{74-84}$Kr, but beyond the shell closure we observe the presence of a possible staggering in ^{88}Kr and ^{92}Kr which deviates quite remarkably from the smooth trend predicted by the GBH model.

To better quantify the agreement between theory and experiment, we have plotted in Fig.2 the theoretical energies of the 2_1^+ (left panel) and 4_1^+ (right panel) as a function of the experimental ones. In the case of perfect match theory/experiment the points should lie on the diagonal line.

As already seen in Fig. 1, the energies of the 2_1^+ are fairly well reproduced by UNEDF0 and UNEDF1, with most of the points falling within ± 200 keV from the experimental value. This value has not been obtained by any rigorous error analysis [29] and it should be considered only as a visual help for the reader to estimate the scattering of the data. The results obtained with UNEDF1$_{SO}$ manifest somehow larger discrepancies, in particular it has the tendency to systematically underestimate the energy of the 2_1^+ state. Similar conclusion holds for the 4_1^+, we observe that the UNEDF0 data are most of the time quite close to the experimental data.
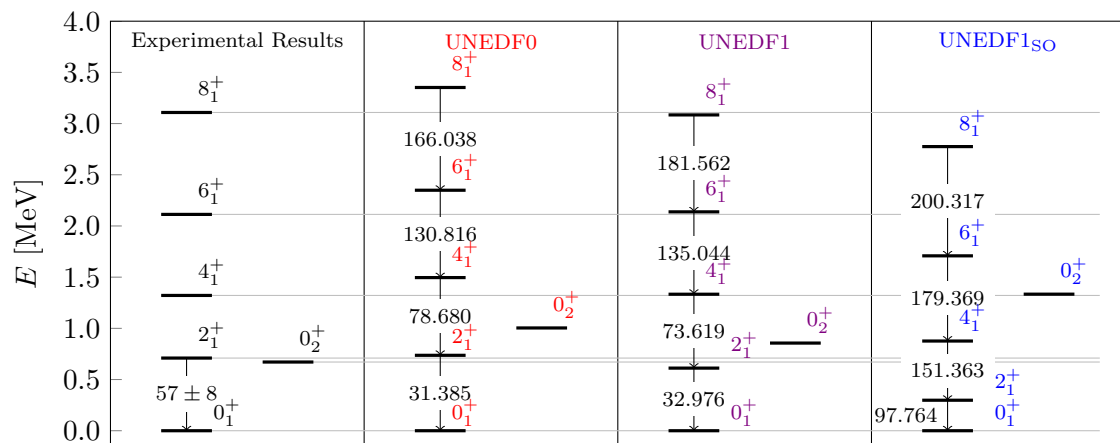

Figure 3. (Colour Online) Shows the $B\left(E2 : 2_1^+ \rightarrow 0_1^+\right)$ (left panel) and $B\left(E2 : 4_1^+ \rightarrow 2_1^+\right)$ (right panel) transition probabilities [28] across the Krypton isotopic chain for the 3 UNEDF functionals represented by hollow: circles for UNEDF0; squares for UNEDF1 and triangles for UNEDF1$_{SO}$.

Having validated the overall quality of GBH methods based on Skyrme functionals, we now discuss in more detail the structure of neutron deficient Kr isotopes. In Fig. 4, we show the potential energy surfaces (PES) as obtained by solving constrained HFB equations at various points in the β, γ plane. The absolute energy minimum is indicated by a dot. UNEDF0 predicts the ^{72}Kr to be slightly oblate and the two other isotopes $^{74-76}$Kr spherical. It is important to notice here that the PES is quite flat along the γ direction and we observe the appearance of secondary energy minima at prolate configurations at $\beta \approx 0.4$. For UNEDF1, we observe a more clear oblate minimum at $\beta \approx 0.3$ in ^{72}Kr, that reduces to $\beta \approx 0.1$ in ^{74}Kr and becoming spherical in ^{76}Kr. As seen for the UNEDF0 functional, also in this case we observe a well marked secondary minimum at $\beta \approx 0.45$ for all three nuclei. The case of UNEDF1$_{SO}$ is quite different, since the energy minimum on the PES is always on the prolate side for all 3 nuclei with $\beta \approx 0.45$. In ^{72}Kr we observe a secondary minimum in the oblate region. In all cases, all functionals provide some softness toward triaxial configurations, although there are no real triaxial minima.

It is interesting to compare these PES with the one produced in Ref [17]. In this case the authors have used the Gogny D1S interaction [30]. A clear triaxial secondary minimum is observed in ^{72}Kr, while here none of the used UNEDF functionals provide such a configuration. The experimental spectrum of ^{72}Kr Fig. 5 is reproduced almost perfectly using the UNEDF1 functional, apart from a small deviation of 0.19 MeV of the second 0_2^+ compared to experimental findings. The UNEDF0 and UNEDF1$_{SO}$ functionals give a slightly low (high) level density of the excited states. Compared to the Gogny spectrum reported in Ref. [17], we observe that the UNEDF functionals give on average a better description of the position of the energy states, although the $B\left(E2\right)$ are not well reproduced for the $B\left(E2 : 2_1^+ \rightarrow 0_1^+\right)$ transition however are reproduced much better for the $B\left(E2 : 4_1^+ \rightarrow 2_1^+\right)$ as illustrated by Fig 3.
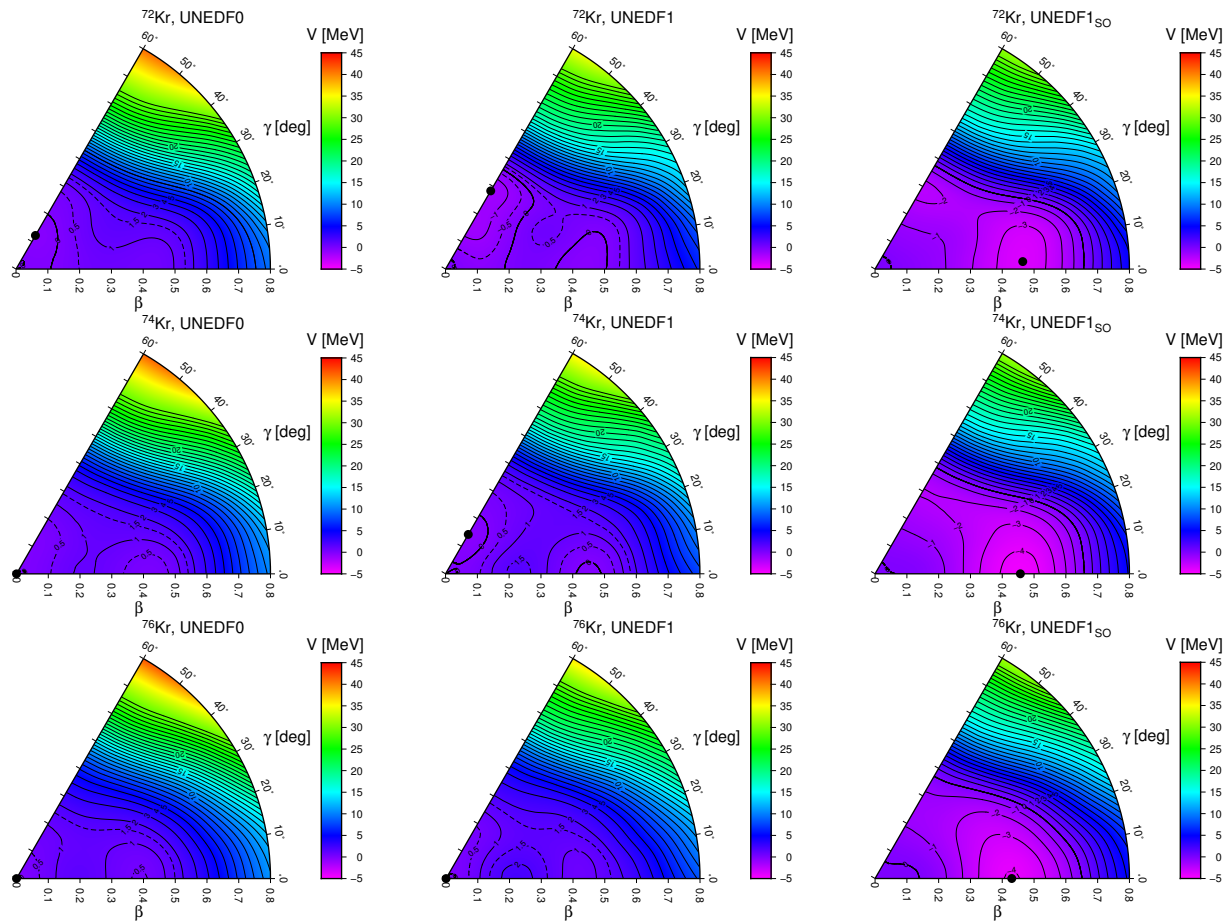
Figure 4. (Colour Online) Potential energy surfaces for ^{72}Kr, ^{74}Kr and ^{76}Kr obtained using UNEDF0, UNEDF1 and UNEDF1$_{SO}$ functionals.

Figure 5. (Colour Online) Shows the energy spectra for a number of low-lying states and their associated $B(E2)$ transition probabilities for ^{72}Kr where we show the experimental results [28] (far left panel), UNEDF0 (left centre panel), UNEDF1 (right centre panel) and UNEDF1$_{SO}$ (far right panel).

4. Conclusion and Discussion

We have analysed the evolution of the low-lying 2_1^+ and 4_1^+ states in the Kr isotopes using the Generalised Bohr Hamiltonian formalism. By using 3 different Skyrme functionals, we have observed that the UNEDF0 and UNEDF1 functionals are able to provide, on average, quite a good description of both energy states and electromagnetic transitions. We have studied in more detail 3 neutron deficient Kr isotopes, namely $^{72-76}$Kr. We have investigated the structure of their PES obtained with the various functionals and we have observed some softness against triaxial deformation in ^{72}Kr, although we see no clear energy minimum as in the Gogny case. By comparing the detailed structure of the full energy spectrum of ^{72}Kr with the current experimental data, we have found that UNEDF1 gives a very nice reproduction of the spectrum. In general we have observed that both UNEDF0 and UNEDF1 seem to provide a fairly good description of Kr isotopes. Similar conclusions were also found in Ref. [14] for the Xe isotopes. These results provide the motivation for a more systematic analysis of nuclear spectra using GBH together with these functionals to assess their quality in reproducing the data.

References
[1] Bender M, Heenen P H and Reinhard P G 2003 *Reviews of Modern Physics* **75** 121
[2] Goriely S, Chamel N and Pearson J 2009 *Physical Review Letters* **102** 152503
[3] Goriely S, Hilaire S, Girod M and Péru S 2009 *Physical Review Letters* **102** 242501
[4] Bertsch G, Girod M, Hilaire S, Delaroche J P, Goutte H and Péru S 2007 *Physical Review Letters* **99** 032502
[5] Sabbey B, Bender M, Bertsch G and Heenen P H 2007 *Physical Review C* **75** 044305
[6] Scamps G and Lacroix D 2013 *Physical Review C* **88** 044310
[7] Sheikh J, Dobaczewski J, Ring P, Robledo L and Yannouleas C 2019 *arXiv preprint arXiv:1901.06992*
[8] Bohr A 1952 *Dan. Vidensk. Selsk* **26**
[9] Próchniak L and Rohoziński S 2009 *Journal of Physics G: Nuclear and Particle Physics* **36** 123101
[10] Perú S and Martini M 2014 *The European Physical Journal A* **50** 88
[11] Matsuyanagi K *et al.* 2016 *Physica Scripta* **91** 063014
[12] Ring P and Schuck P 2004 *The nuclear many-body problem* (Springer Science & Business Media)
[13] Duguet T, Bender M, Bennaceur K, Lacroix D and Lesinski T 2009 *Physical Review C* **79** 044320
[14] Prochniak L 2015 *Physica Scripta* **90** 114005
[15] Skyrme T 1958 *Nuclear Physics* **9** 615–634
[16] Clément E *et al.* 2007 *Physical Review C* **75** 054313
[17] Girod M, Delaroche J P, Görgen A and Obertelli A 2009 *Physics Letters B* **676** 39–43
[18] Rodríguez T R 2014 *Physical Review C* **90** 034306
[19] Fu Y, Mei H, Xiang J, Li Z, Yao J and Meng J 2013 *Physical Review C* **87** 054305
[20] Heyde K and Wood J L 2011 *Reviews of Modern Physics* **83** 1467
[21] Rowe D J and Wood J L 2010 *Fundamentals of nuclear models: foundational models* (World Scientific Publishing Company)
[22] Dobaczewski J *et al.* 2009 *Computer Physics Communications* **180** 2361–2391
[23] Girod M and Grammaticos B 1979 *Nuclear Physics A* **330** 40–52
[24] Baran A, Sheikh J, Dobaczewski J, Nazarewicz W and Staszczak A 2011 *Physical Review C* **84** 054321
[25] Kortelainen M, Lesinski T, Moré J, Nazarewicz W, Sarich J, Schunck N, Stoitsov M and Wild S 2010 *Physical Review C* **82** 024313
[26] Kortelainen M, McDonnell J, Nazarewicz W, Reinhard P G, Sarich J, Schunck N, Stoitsov M and Wild S 2012 *Physical Review C* **85** 024304
[27] Shi Y, Dobaczewski J, Greenlees P *et al.* 2014 *Physical Review C* **89** 034309
[28] National Nuclear Data Center, Brookhaven National Laboratory `http://www.nndc.bnl.gov/`
[29] Dobaczewski J, Nazarewicz W and Reinhard P 2014 *Journal of Physics G:* **41** 074001
[30] Decharqé J and Gogny D 1980 *Physical Review C* **21** 1568